DOI: 10.1002/anie.200906928

Biosensors

Gold Nanoparticle–Fluorophore Complexes: Sensitive and Discerning "Noses" for Biosystems Sensing

Uwe H. F. Bunz and Vincent M. Rotello**

biosensors · displacement assays · fluorescent probes · nanoparticles

Gold nanoparticles (NPs) efficiently quench adsorbed fluorophores. Upon disruption of such complexes by an analyte, fluorescence turn-on is observed. By judicious choice of the functionalized NP and the fluorophore, these complexes display different responses to analytes, thus leading to versatile yet simple array-based sensor platforms. Using this strategy, we can identify proteins in buffer and serum, distinguish between both different species and different strains of bacteria, and differentiate between healthy, cancerous, and metastatic human and murine cells.

1. Introduction

The detection and quantification of cells, proteins, and other biosystems in complex matrices is important for disease detection. There is a wealth of methods available to attain this goal, including antibodies used in ELISA-type tests, proteomics and related approaches coupled with mass spectrometry, as well as widely employed techniques such as gel electrophoresis to detect serum imbalances in patients with liver failure or other gross metabolic problems.[1] For the detection of microorganisms, plating and culturing as well as PCR are standard; viral infections are generally detected by ELISA-type tests, or in the case of early detection of HIV also by PCR.[2] Other methods for the detection of microorganisms, including electrochemical assays, have been suggested.[3] However, the field is open when it comes to simple and rapid assays that indicate the presence of an analyte by color or fluorescence change; in such a case one "strip" might even contain a small library of indicators, the combined responses of which would indicate the presence or absence of specific analytes.

The combination of selective instead of specific sensors or indicators into a sensor array generates a chemical nose or tongue, in which the combined response of the library identifies analytes or disease states. Often, the terms "chemical tongue" and "chemical nose" are applied to selective electrodes and electrochemical detection of analytes.[4] While these methods are valuable, this Minireview will focus upon optical detection methods, that is, materials that give a fluorescence signal. Closely related to this topic are small libraries of dyes that give colorimetric changes upon exposure to analytes. Attractive examples for the detection of a diverse set of analytes are found in the Suslick group's sensors using indicator arrays,[5] as well as in Anslyn and Hewage's recent artful work using a minilibrary of thiol-functionalized squaraine dyes to detect metal cations.[6] The transduction mechanism of such small libraries can vary; in the case of Suslick's sensors, a series of solvatochromic dyes changes color upon exposure to analytes. However, a number of cross-reactive,[7] but not very selective, sensor molecules can also be envisioned that function as a displacement assay, in which a complex is disrupted by an analyte.[8,9] In indicator displacement assays (IDAs), an entity containing one or many recognition elements is combined with a signal-generating entity, typically a colorimetric species or a fluorescent molecule. Upon combination of the dye with the recognition entity, a self-assembled "supramolecular" complex forms. This complex is subjected to the solution of an analyte, which replaces some or all of the dye from the recognition element to generate a signal.

In a classical sensor or indicator, the recognition element is covalently attached to the signal-generating unit. Binding of an analyte will induce a change in the electronics of the dye and therefore lead to red- or blue-shifted absorption and/or emission.[10] The advantage of IDAs over classical assays is their mix-and-match character, that is, a series of n receptor units can be combined with a second series of m indicator molecules to form a matrix $n \times m$ of self-assembled IDAs. Consequently, the synthetic effort to prepare a sensor library

[*] Prof. U. H. F. Bunz
School of Chemistry and Biochemistry
Georgia Institute of Technology
901 Atlantic Drive, Atlanta GA 30332 (USA)
Fax: (+1) 404-385-1795
E-mail: uwe.bunz@chemistry.gatech.edu
Prof. V. M. Rotello
Department of Chemistry, University of Massachusetts
710 N Pleasant Street, Amherst, MA (USA)
E-mail: rotello@chem.umass.edu

of any size is lower than to prepare each new sensor by synthesizing it. Furthermore, each of the two components of an IDA can be independently changed to manipulate binding affinities and selectivities of the formed IDAs.

Suspensions of gold nanoparticles (NPs)[11] are deeply colored; their monolayer-protected and enhanced derivatives have found widespread applications in biological assays.[12] Gold NPs are excellent quenchers of fluorescence, working either by a FRET (fluorescence resonance energy transfer) or electron-transfer type mechanism; NPs can be obtained in sizes from 2 to 50 nm. Monolayers[13] of ligands confer differential solubility to NPs in any desired solvent and can contain sensory or molecular-recognition appendages. The monolayer molecules featuring thiol end groups are anchored on the NPs by a ligand exchange process, with the gold–sulfur bond anchoring the monolayers. As a consequence, combination of NPs with different thiol ligands gives access to a large variety of functionalized NP-based quenchers of different sizes, with different recognition elements and inherent polyvalent abilities.[14,15] Taken together, the charge and hydrophobicity of the monolayers and therefore the charge and hydrophobicity of the protected NPs can be varied at will.

Monolayer-protected gold NPs are polyvalent by design and can be combined with any type of fluorophore. However, we cover herein IDAs that result when positively charged gold NPs are combined with negatively charged conjugated polymers of the poly(*para*-phenyleneethynylene) (PPE) type and with the likewise anionic green fluorescent protein (GFP, Figure 1). In both cases, the combination of polyvalent fluorophore with the polyvalent gold NP generates attractive self-assembled IDA sensors that discern proteins, bacteria, and cells by analyte-induced fluorescence turn-on. Gold is not the only possible material for this sensing approach; in the last part of this Minireview we will show that cobalt–ferrite NP–PPE constructs are also useful for IDA detection of pyrophosphate (PPi) in the presence of phosphate (Pi) anions.

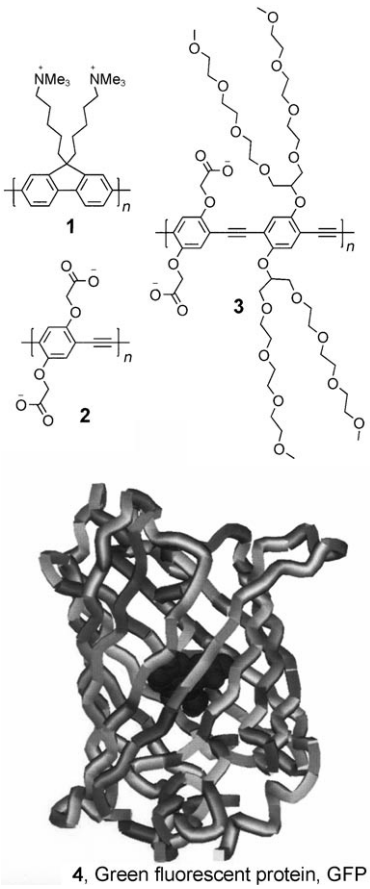

Figure 1. Fluorophores **1**–**4**.

2. Interaction of Gold NPs with Conjugated Polymers

2.1. Gold NPs as Powerful Fluorescence Quenchers

Heeger, Bazan, and co-workers[16] discovered that the fluorescence of cationic, water-soluble polyfluorene **1** (Figure 1) is quenched by the addition of minute amounts of gold NPs of different sizes. These NPs display apparent Stern–Volmer constants (K_{sv}) that are in the range of $K_{sv} = 10^7$–10^{11}. The mechanism of the quenching (electron transfer vs. energy transfer) of **1** by the NPs could not be determined with certainty, even though there is a significant spectral overlap of the emissive features of **1** with the absorption spectra of the NPs, suggesting the occurrence of FRET. The authors assumed that the quenching occurs by a static mechanism, which is generally the case as the emissive lifetimes of conjugated polymers such as **1**–**3** are in the range of 0.3–0.7 ns. Under these conditions, the observed Stern–Volmer constants equate to a binding constant K_a. Diffusion-controlled or dynamic quenching will play only a minor role at the

Uwe Bunz (1963) earned his Dr. rer. nat. in 1990 from the LMU Munich; after a postdoctoral stint at UC Berkeley with K. P. C. Vollhardt, he completed his Habilitation (Dr. rer. nat. habil.) with K. Müllen at the MPI for Polymer Research in Mainz. From 1997–2003 he was Associate and then Full Professor at the University of South Carolina. Since 2003 he has been Professor of Chemistry at the Georgia Institute of Technology. His research interest is in conjugated polymers.

Vincent Rotello (1964) earned his Ph.D. in 1990 from Yale University; after a postdoctoral stint at MIT with J. Rebek, Jr., he joined the Department of Chemistry at the University of Massachusetts Amherst in 1992, where he rose through the ranks. Since 2003 he has been the Goessmann Professor of Chemistry. His research interest is in nanoparticles and interfacial engineering.

micromolar polymer concentrations used in these studies. The Stern–Volmer equation [Eq. (1); I_0 is the initial fluorescence

$$I_0/I_{[Q]} = 1 + K_{SV}[Q] \quad (1)$$

intensity and $I_{[Q]}$ is the fluorescence intensity after addition of the quencher Q] therefore provides a convenient tool for the determination of binding constants. The obtained quenching data need to be fitted to this linear equation. The team of Heeger and Bazan extracted high apparent Stern–Volmer constants (K_{sv}) from the data but also noted that the quenching curves were not linear but curved upwards.

Why is that? In the Stern–Volmer equation, $[Q]$ represents the concentration of free quencher (Q) and not the total concentration of quencher $[Q]_{tot}$. However, $[Q]$ is difficult to measure, while $[Q]_{tot}$ is just the concentration of added quencher. In cases where $K_{sv}[\text{fluorophore}] < 1$, the assumption $[Q] \approx [Q]_{tot}$ is justified and will generally give linear quenching data.[17] However, in cases where $K_{sv}[\text{fluorophore}] \gg 1$, this assumption breaks down, and $[Q] \ll [Q]_{tot}$. In such cases Equation (2) will have to be used to extract a valid K_{sv} or K_a from the quenching data.

$$I_{[Q]} = I_0 + \frac{\alpha}{2}\left[\left([F]_0 + n[Q]_{tot} + \frac{1}{K_{SV}}\right) - \left\{\left([F]_0 + n[Q]_{tot} + \frac{1}{K_{SV}}\right)^2 - 4n[F]_0[Q]_{tot}\right\}^{1/2}\right] \quad (2)$$

2.2. Influence of Hydrophobicity and Charge upon the Binding of Conjugated Polymers of the PPE Type to Monolayer-Protected NPs[18]

How is the binding between conjugated polymers and gold NPs influenced by the structures of the conjugated polymer and the monolayer that protects the gold NP? To get a systematic understanding, we have restricted our studies to the two anionic PPEs **2** and **3**. The attachment of the branched oligo(ethylene glycol) side chains to the PPE backbone increases the fluorescence of **3** as compared to that of **2** by a factor of four and also minimizes any nonspecific interactions with biological matter, an important concern in our sensor designs. Additional versatility is provided through the use of GFP **4**, a negatively charged, emissive protein. For simplicity, all of the used fluorophores and the structures of monolayer-protected, 2 nm NPs are shown in Figure 1 and Figure 2.

To investigate the fundamental interactions between gold NPs and conjugated polymers, we selected the simple PPE **3**[19,20] and obtained the binding constants between **3** and **NP1**–**11** in aqueous solution with different salt concentrations. The binding constants between **3** and the NPs were obtained by fluorescence quenching of **3** by **NP1**–**11** and analysis of the obtained data using Equation (2). Figure 3 shows the results of the binding experiments in the presence of varying concentrations of sodium chloride.

Aromatic-monolayer-functionalized NPs are more effective in fluorescence quenching and therefore bind more strongly to the conjugated polymer **3** than the aliphatic NPs. However, in the case of the aliphatic NPs, the most hydrophobic NP (**NP6**) is the one that binds most strongly to **3**. A second trend is the sensitivity of the binding constants to the presence of salt. As many biological processes occur in an environment with high ionic strength, its influence on the binding of **3** to NPs had to be evaluated at varying salt concentrations.

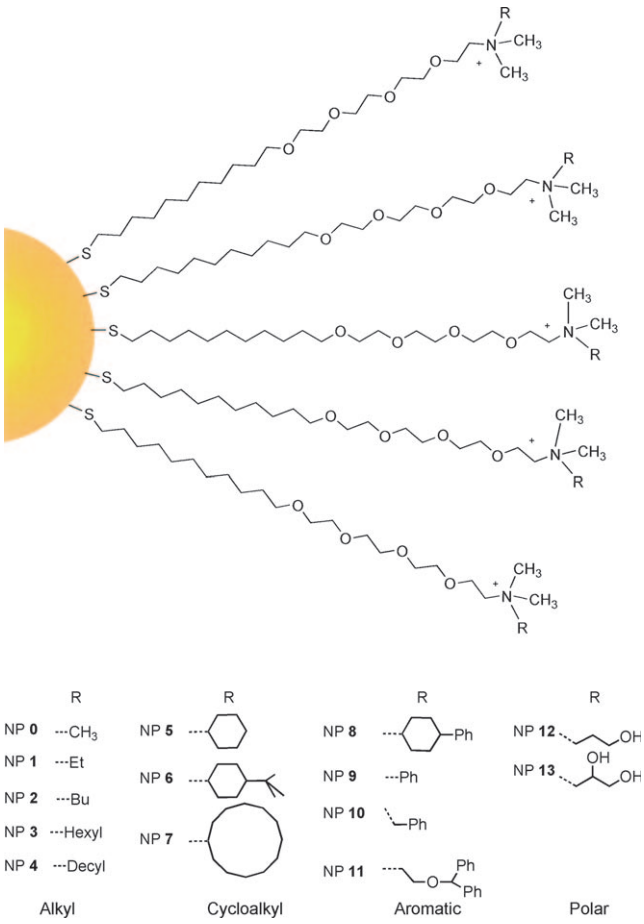

Figure 2. Monolayer-functionalized gold NPs **NP0**-**NP13**.

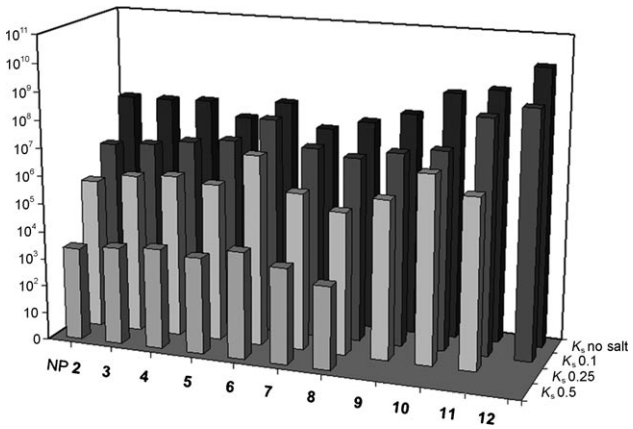

Figure 3. Logarithmic plot of binding constants between **NP1**–**NP11** and PPE **3** in water and in 0.1, 0.25, and 0.5 M saline solution ($K_s = K_{SV} = K_a$). Figure reproduced with permission from reference [18].

The binding between NPs and **3** has hydrophobic and electrostatic components. Increasing salt concentration should, at least at first glance, disrupt the latter but leave the former intact. Matters seem more complicated, as the most hydrophobic NPs functionalized by aromatic monolayers show the largest binding constants in pure water but are also the ones that are most sensitive towards disruption by increasing salt concentration. This effect might be due to a disruption of the weak binding between the π face of the polymer and the cationic head groups (cation–π interaction).[21]

For further analysis, we correlated the hydrophobicity of the ligands (as determined by the partition coefficient) with the binding constants (K_a) obtained from the titration of the gold NPs with **3** (Figure 4). It is interesting to note that the

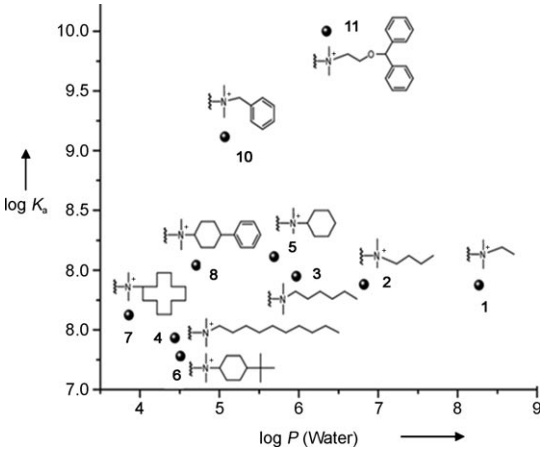

Figure 4. Logarithmic relation of binding constants (K_a, NP-**3**) and partition coefficient of **NP1**–**NP11** (**NP9** is not plotted owing to the force-field interaction). Figure reproduced with permission from reference [18].

hydrophobicity does not play a large role for the binding in the case of the alkyl-substituted ammonium-functionalized gold NPs. Their increased hydrophobicity does not result in an increased binding constant. This effect might be due to a concomitant decrease in the electrostatic interactions between cationic gold NPs and PPE **3**. In the case of the aromatic ammonium-functionalized gold NPs, K_a is correlated to the hydrophobicity. The more hydrophobic the ligands around the gold NP, the higher the binding constant for the attachment to the PPE **3**. This result is understandable, as strong aromatic–aromatic interactions between gold NPs and the PPE will increase their tendency to bind. However, there must be a strong electrostatic component present, as the constructs that are formed between **3** and NPs with aromatic ammonium side chains are easily disrupted at increasing salt concentration. At physiological salt concentrations, the binding is weakened for NPs displaying an aromatic ammonium head group, but with $K_a = 10^6$–10^7 it is still sufficiently strong for these constructs to be used successfully in the displacement assays. If higher binding constants are desired, the PPE **2** with higher charge density also shows higher binding constants, as demonstrated in the case of the titration of **NP3** with **2**, where $K_a = 1.7 \times 10^8$ as compared to $K_a = 8.8 \times 10^7$ for titration of **NP3** with **3**. Figure 5 displays representative titration curves and a binding trace obtained from the interaction of **NP3** with **2**.

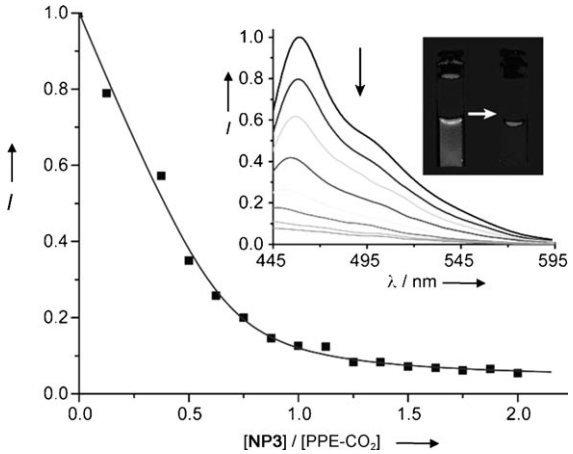

Figure 5. Fluorescence intensity changes of **2** (100 nM) at 465 nm upon addition of cationic NP**3**. Inset shows the fluorescence spectra and the images of solutions of **2** before and after addition of NP**3.** Figure reproduced with permission from reference [22].

3. Detection of Proteins Using Gold NP–Fluorophore Constructs

3.1. Detection of Proteins by Constructs of PPE and a Library of Six NPs[22]

As a testbed for the ability of the NP–PPE constructs to sense proteins, a small library was generated from the NPs **NP0**,**1**,**3**,**5**,**10**,**12** and the carboxylate PPE **2**. Solutions of the NPs were mixed with a dilute solution of **2** until the fluorescence of the PPE was attenuated to 10 % of its original value (Figure 5 and Figure 6). To this library dilute solutions of the seven proteins shown in Figure 7 were added, and the fluorescence response of the constructs was quantified (Figure 8). Even from the raw data it can be seen that the seven selected analyte proteins induce varied turn-on and turn-off responses in the six NP–PPE constructs. Perhaps not unexpectedly, β-gal displays the largest response on a molar basis, a testimony to its high molecular weight and strong negative charge. Cytochrome C (CC) displays effective quenching, a consequence of the effective FRET from the PPE to the deeply colored protein. Figure 8b shows a linear discriminant analysis (LDA) plot; all seven proteins are well discriminated, and unknowns taken from the training set were identified with 95 % accuracy.

3.2. Detection of Proteins in Serum: Use of Green Fluorescent Protein[23]

The discrimination of proteins by these simple and nonbiological NP–PPE constructs is surprisingly powerful, perhaps because each NP–PPE construct has an analog

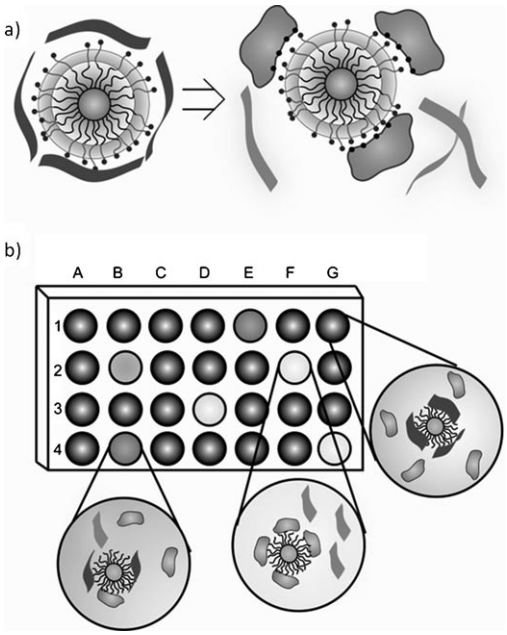

Figure 6. Fluorophore displacement protein sensor array. a) Displacement of quenched fluorescent polymer by protein analyte with concomitant restoration of fluorescence. b) Pattern generation through differential release of fluorescent polymers from gold NPs. Figure reproduced with permission from reference [22].

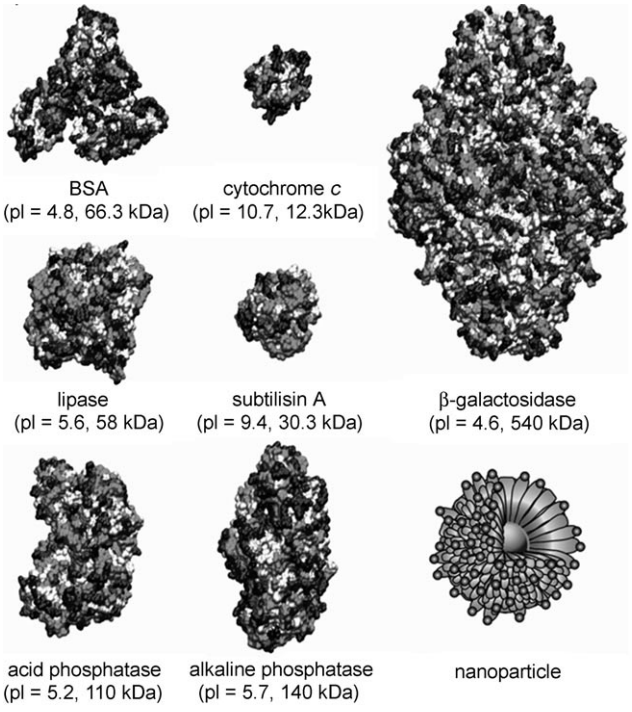

Figure 7. Structural features of target analytes. Relative size, molecular weight, and isoelectric points of seven proteins and the NP used in the sensing study. Figure reproduced with permission from reference [22].

response towards each protein, that is, if it is assumed that each fluorescence response can give on the order of 1000 different discernible values, there would be a theoretical response space that is constructed from $1000^6 = 10^{18}$ different

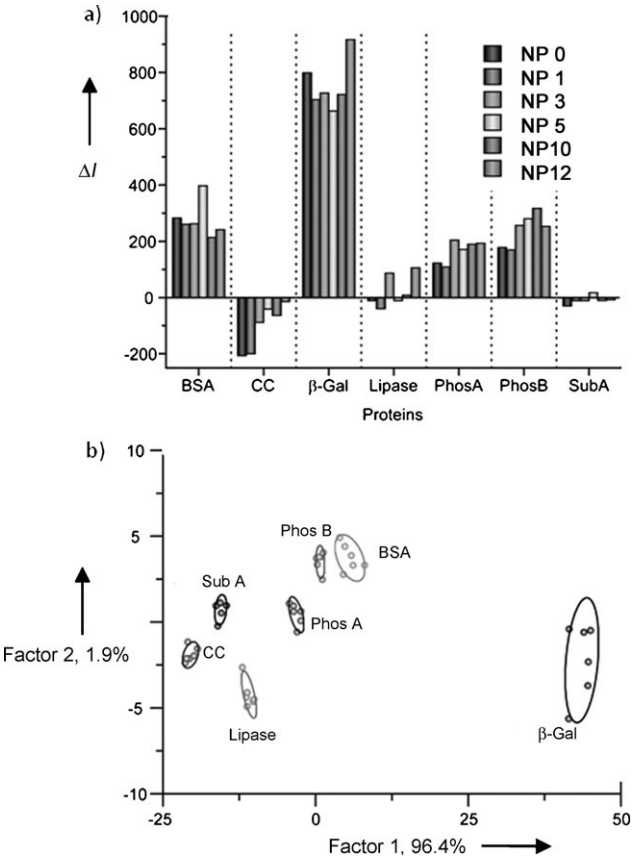

Figure 8. Array-based sensing of protein analytes at 5 μM. a) Fluorescence response (ΔI) patterns of the NP–PPE sensor array (**NP0,1,3,5,10,12**) against various proteins (CC: cytochrome c, β-Gal: β-galactosidase, PhosA: acid phosphatase, PhosB: alkaline phosphatase, SubA: subtilisin A). Each value is an average of six parallel measurements. b) Canonical score plot for the first two factors of simplified fluorescence response patterns obtained with NP-PPE assembly arrays against 5 μM proteins. The canonical scores were calculated by LDA for the identification of seven proteins. The 95% confidence ellipses for the individual proteins are also shown. Figure reproduced with permission from reference [22].

response elements, reduced somewhat by the fact that not all responses are independent. Sensing of single proteins in water, albeit of fundamental interest, is not sufficient to use these types of constructs to determine analytes in complex matrices such as serum, sperm, urine, or sweat. The most diagnostically important biological matrix is human serum, the proteinacious solution that remains when blood is freed from white and red blood cells.[24] As the plasma/serum proteome contains more than 20000 different proteins, it is the perfect proving ground for any bioanalytical method. To minimize nonspecific interactions between the fluorophore and the serum proteins, green fluorescent protein (GFP) was selected as the fluorophore in the sensing of serum proteins, as PPEs can display nonspecific interactions with different proteins (Figure 9).[25a] Furthermore, GFP has a defined size and molecular weight, and its fluorophore core is embedded in a barrel-shaped protein, thus significantly reducing aggregation-induced quenching and excimer formation that can occur with conjugated polymers.[25b] GFP displays similarly

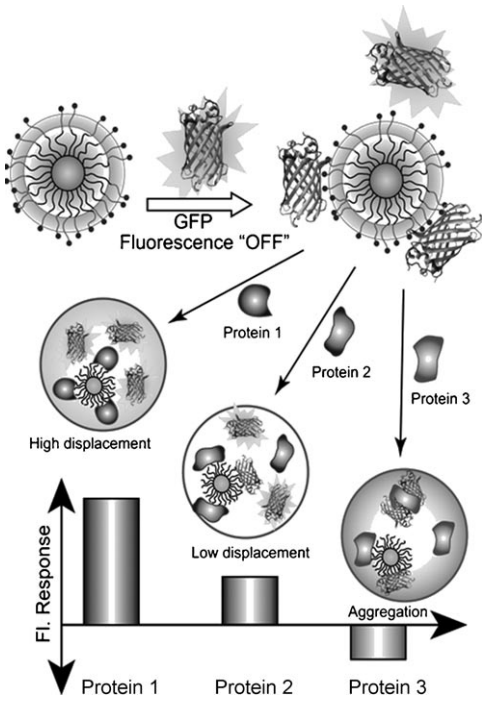

Figure 9. Structural features of an NP and modes of sensor response. Schematic illustration of the competitive binding between protein and quenched GFP–NP complexes and protein aggregation leading to the fluorescence turn-on or further quenching using **NP1**,**3**,**6**,**9**, and **NP13**. Figure reproduced with permission from reference [23].

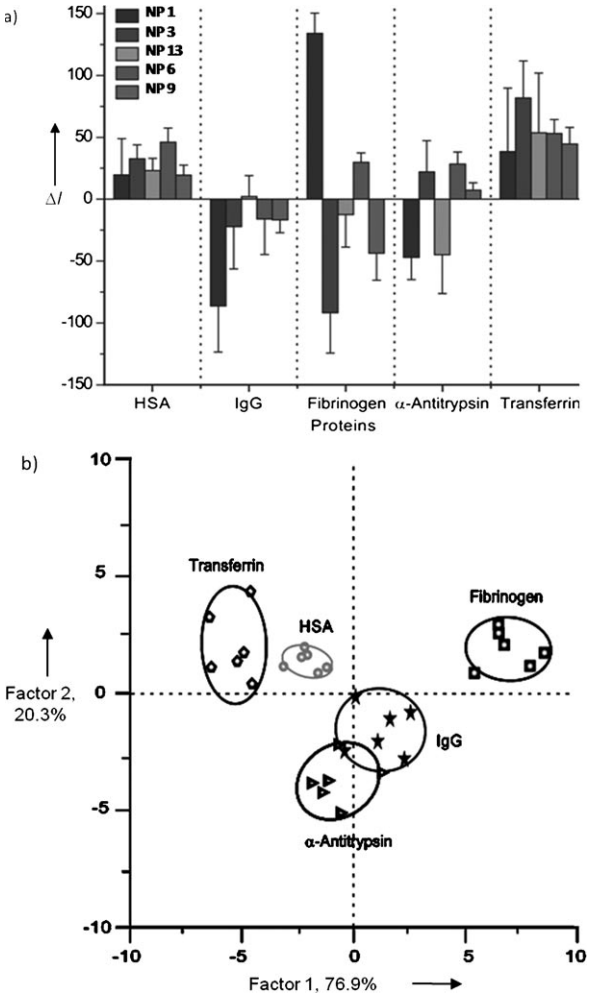

Figure 10. a) Fluorescence response (ΔI) pattern of five GFP–NP adducts in the presence of serum proteins spiked in human serum at 500 nM concentration (responses are the average of six measurements, and error bars are standard deviations of the measurements). b) Canonical score plot for the fluorescence patterns as obtained from LDA against five protein analytes at fixed concentration (500 nM) with 95% confidence ellipses. Figure reproduced with permission from reference [23].

high binding constants to the NPs as the PPEs do. For example, the **NP13**–GFP complex displays a K_a of 5×10^9, similar to that of PPE **3** with **NP10–13**.

The twenty most abundant serum proteins make up 99% of the serum protein content by weight. Of those twenty, the five most abundant ones, albumin (70%), IgG (14%), transferrin (5.7%), fibrinogen (2.8%), and α-antitrypsin (0.7%), cover 93% of the proteinacious mass in human serum. Medicinal diagnostics of serum samples is generally done by simple electrophoresis[1] to determine large-scale protein imbalances in serum that arise for liver malfunction and other disease states, while for the detection of proteins such as troponin, which are present in trace amounts, antibody assays are used. Bridging these methods are 2D-SDS-PAGE[1] electrophoresis and SELDI mass spectrometric methods (SELDI = surface-enhanced laser desorption/ionization).[26] While monoclonal antibodies are very sensitive, they require a specific antibody for each protein; electrophoresis is simple but limited, while mass spectrometry needs expensive instrumentation and sample throughput is not very fast. As a consequence, there is significant interest in alternative fundamental and diagnostic tools that determine the level of specific proteins in serum. To this end, a library of the positively charged **NP1**,**3**,**6**,**9**, and **NP13** was created, and the NPs were combined with the negatively charged GFP in commercially available human serum. A typical ratio of NP/GFP was 2:1 at 500 nM concentration of the NPs to generate complexes with optimum responsivity to added proteins. Figure 10 displays the fluorescence changes of the NP–GFP constructs in serum upon spiking with 500 nM of HSA, IgG, fibrinogen, antitrypsin, and transferrin, respectively. Both fluorescence intensity decrease as well as increase are observed, as depicted. Linear discriminant analysis demonstrates that the proteins, with exception of IgG and antitrypsin, are well-resolved in two dimensions, forming non-overlapping patterns. IgG and antitrypsin, however, are then differentiated in the third dimension (not shown). Further experiments indicated that mixtures of different proteins and the addition of one protein in different concentrations also led to a specific and reproducible change in the LDA-based patterns. Mixtures of proteins spiked into the serum could be detected and gave specific responses.

These results suggest that simple libraries made from differently functionalized gold NPs and either biofluorophores such as GFP or conjugated polymers recognize and detect proteins and protein imbalances in serum as a complex

matrix. This is a significant achievement for these fairly simple constructs, which only employ electrostatic and hydrophobic interactions for the facile detection and quantification of proteins in water, buffer, and serum.

4. Detection of Bacteria and Mammalian Cells Using PPE–NP Constructs

4.1. Interaction of Bacteria with Inorganic NPs

Bacteria, sized around 0.5–10 μm, have negatively charged surfaces that are suitable for interaction with NPs of different shapes. Murphy et al.[27a] demonstrated that CTAB-functionalized gold nanorods or nanospheres (Figure 11; CTAB = cetyltrimethylammonium bromide) assemble homogeneously on the coats of *B. cereus*. The teichoic acid residues make this Gram-positive microorganism highly negatively charged, thus promoting electrostatic bonds to cationic materials.

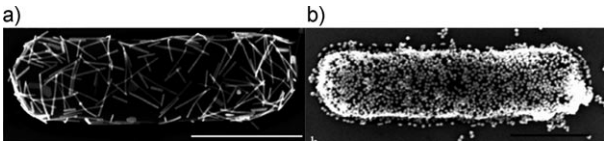

Figure 11. a) Monolayer of gold nanorods (25 nm × 400 nm) after 15 min. b) Gold nanospheres (45 nm diameter) on *Bacillus cereus* after 15 min deposition. Scale bars are 1 μm. Figure reproduced with permission from reference [27a].

In other cases, mannose-substituted gold NPs were specifically complexed by the pili, that is, the fine "hairs" that emanate from the surface of *E. coli* bacteria. The pili are rich in lectins (sugar-binding proteins) and therefore interact preferentially with these parts of the bacterial anatomy.[28] In a study by Bertozzi and Bednarski, a mannose–biotin construct was assembled by avidin and combined with *E. coli* bacteria.[27b] An avidin antibody was added, and the formed construct was incubated with protein A functionalized gold NPs. This strategy allowed the visualization of functional mannose-binding groups on the pili by the gold NPs using TEM. In a similar vein, gold nanorods were functionalized by electrostatic interactions or through covalent attachment with an antibody against *P. aeruginosa*. Incubation with these bacteria led to hybrids, in which the nanorods covered the bacterial surface.[29] However, the interaction of fluorophore–NP constructs with bacteria had not been exploited, though the groups of Swager and Bunz have investigated the interaction of conjugated polymers with bacteria.[30,31]

The successful exploitation of protein sensing suggested that the functionality on bacterial surfaces should respond to nanoconstructs formed from gold NPs and PPEs such as **2** or **3**. Bacterial cell walls are negatively charged and should furnish a polyvalent environment that can interact strongly with NP–PPE constructs under fluorescence turn-on, similarly to the effect that was observed for the proteins. The published papers strongly suggest success for this approach.[27–29]

4.2. Detection of Bacteria[32]

Detection and quantification of bacteria is important in clinical, environmental, and public health sectors; bacterial infections are involved in food poisoning, hospital-acquired infections, and other areas that are of great concern for public health. In clinical diagnostics, bacterial infections are identified by plating and culturing, an efficient method that is, however, quite time-consuming. While several high-tech methods, including PCR, have been used to detect specific microorganisms,[33] a facile wet-chemical method for the speedy detection and identification of microorganisms would be of interest in both a clinical setting as well to test for food spoilage.[34] According to Reisner and Woods,[35] more than 80% of all clinically reported infections are caused by only seven microorganisms, *E. coli* and *S. aureus* accounting for approximately half of all.

The three hydrophobic particles **NP3**,**5**,**10** were combined with the PPE **3** to give constructs in which the PPE's fluorescence was quenched to 10% of its original value (Figure 12). These solutions were combined with bacterial preparations that had an optical density of 0.05 at 600 nm. After several minutes of exposure, the bacterial cells replaced a fraction of PPE **3** from the NPs, and a significant fluorescence turn-on occurred in most cases. Twelve different bacterial species or strains were investigated; Figure 13 displays the raw fluorescence responses that the constructs experienced upon exposure to the respective bacteria. It is important to note that the three NPs all display hydrophobic head groups. Attempts to disrupt conjugates in which hydrophilic or short-chain ammonium salts were involved, such as **NP0**,**1**,**12**,**13**, were not successful, and the reported fluorescence recovery was close to zero. From Figure 13 it can be seen that the twelve bacteria could be readily discerned by the

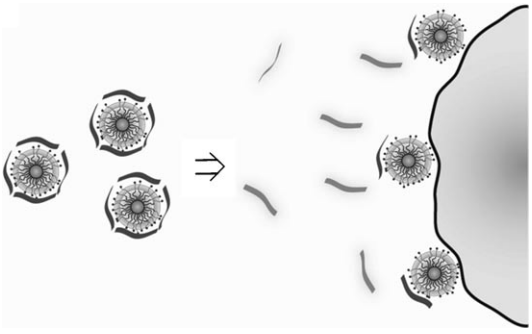

Figure 12. Schematic representation of the displacement of anionic conjugated polymers from cationic NPs by negatively charged bacterial surfaces. In the case of release from the NP, the initially quenched π-conjugated polymers regain their fluorescence. The fluorescence response is dependent upon the level of displacement determined by the relative binding strength of polymer–NP and bacteria–NP interactions. By modulating such interactions, the sensor array may generate distinct response patterns for different bacteria. Figure reproduced with permission from reference [32].

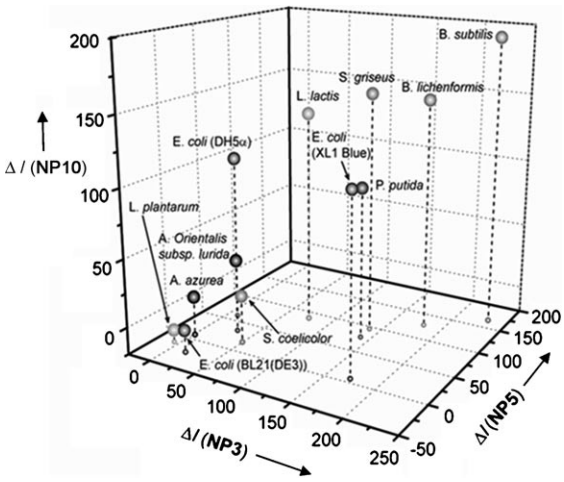

Figure 13. Fluorescence response patterns of NP–polymer constructs in the presence of various bacteria ($OD_{600} = 0.05$). Histograms of fluorescence intensity changes. Three-dimensional representation of the fluorescence intensity changes against the three NP–polymer constructs. Each value is an average of six parallel measurements. Figure reproduced with permission from reference [32].

three NPs used. Figure 14 shows the LDA plot of the same data. All twelve microorganisms group distinctly. Importantly, three different *E. coli* strains (XL1 Blue, BL21(DE3), DH5α) were easily discerned. The three strains were not grouped particularly closely together by their fluorescence responses, which suggests that there must be some differences in their surface chemistries. Also, Gram-negative (*E. coli*, *P. putida*) and Gram-positive bacteria (*A. azurea*, *B. subtilis*, *B. lichenformis*) could easily be discerned but were also not grouped in any particular way in the LDA plot (Figure 14). Random solutions of bacteria from the training set were identified in 95% of all cases, thus demonstrating the robustness of this small NP–PPE library. It is speculated that hydrophobic hotspots on the surface of the bacteria are a reason for their binding to hydrophobic NPs, and while there is significant

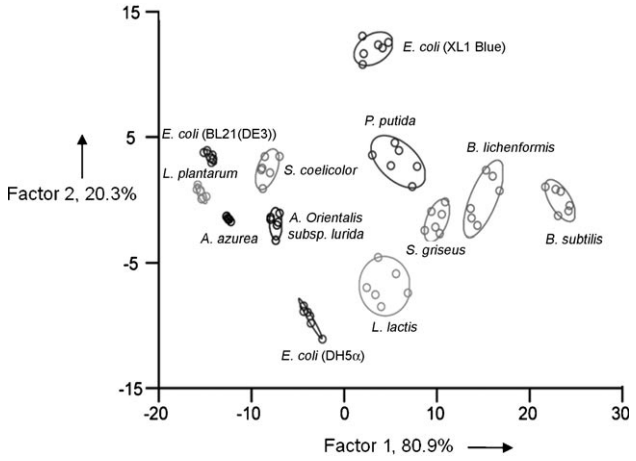

Figure 14. Canonical score plot for the fluorescence response patterns as determined with LDA. The first two factors consist of 96.2% variance, and the 95% confidence ellipses for the individual bacteria are depicted. Figure reproduced with permission from reference [32].

literature on the function of bacterial surface proteins and surface structure, the mesoscopic landscape of the bacterial surface, that is, how the protein complexes, lipid rafts, and glycans self-organize into structures that are 10–100 nm in size, is much less known but probably plays a significant role for the surprising success of this simple NP–PPE-based assay.

4.3. Detection of Mammalian Cells[36]

The successful detection and identification of bacteria by the preformed NP–fluorescent polymer complexes presents the possibility that mammalian cells might also be identified. An obviously important question is if cancerous cells would give different responses to the NP fluorophore constructs than normal cells would. Furthermore, could this type of assay distinguish between cancerous and metastatic cells? Mammalian cells and their interactions with gold NP–fluorophore constructs were studied to differentiate normal from cancerous and metastatic cells and also to differentiate cancerous and metastatic cells. A successful differentiation would generate potential tools for the development of simple assays for the early diagnosis of neoplastic growth and its classification into metastatic or nonmetastatic cells.

To test the ability of our sensors to discriminate mammalian cells, we investigated a series of cell lines (Table 1) and subjected them to the constructs formed from **NP5**,**10**,**12** and

Table 1: List of the used mammalian cells.

Species	Organ	Cell Line	State
human	liver	HepG2	cancerous
	cervix	HeLa	cancerous
	testis	NT2	cancerous
	breast	MCF10A	normal
		MCF-7	cancerous
		MDA-MB-231	metastatic
mouse	BALB/c breast	CDBgeo	normal
		TD	cancerous
		V14	metastatic

PPE **2**. These three NPs in combination with PPE **2** generated the largest responses towards mammalian cells (Figure 15, Figure 16) and were obtained from the library shown in Figure 2; other NPs were tested but did not show significant responses when exposed to mammalian cells.

The three NP–PPE constructs are able to differentiate between four different human cancer cell lines but are also capable of discerning breast tissue that is either normal, cancerous, or metastatic. These results were promising; however, all of the cell lines were harvested from different individuals. So what is observed may not necessarily derive from different stages of a specific cell type but could also be an expression of genetic differences of the individuals that contributed the cells. To exclude this possibility, a set of isogenic cell lines were investigated. These were obtained from BALB/c mice breast tissue and consisted of healthy cells as well as transformed cell lines, which result in non-invasive and invasive tumors when transplanted into mice. The use of

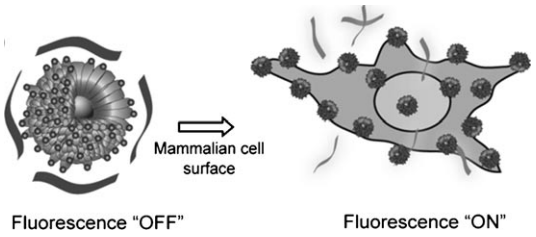

Figure 15. Schematic depiction of the fluorophore-displacement cell-detection array. Displacement of quenched fluorescent polymer (dark strips, fluorescence off; light strips, fluorescence on) by a cell with concomitant restoration of fluorescence.

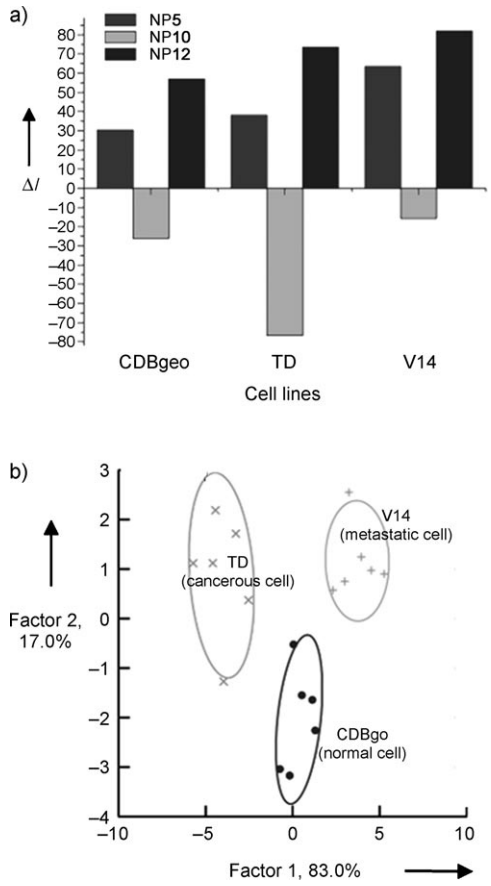

Figure 16. a) Detection of isogenic cell types. Change in fluorescence intensities for three cell lines of same genotype CDBgeo, TD cell, and V14 using NP–polymer supramolecular complexes. Each value is averaged over parallel measurements. b) Canonical score plot for the first two factors of simplified fluorescence response patterns obtained with NP–PPE assembly arrays against different mammalian cell types. Figure reproduced with permission from reference [36].

isogenic cell lines is a particularly stringent test for the development of diagnostic tools, as the cells all share the same genotype; therefore, only changes arising from the state of the cell, that is, healthy, cancerous, or metastatic, result. Figure 16 shows that with the three NP–PPE constructs the isogenic cell lines were distinguished both by inspection of the fluorescence responses and, more dramatically, in the LDA plot.

Figure 17 displays a canonical score plot for the fluorescence response patterns for all of the observed responses of breast cells from humans and mice. The LDA plot differentiates metastatic from cancerous and normal cells. Interestingly, the normal cells CDBgeo and MCF10A can not be distinguished, yet all the other cell types are surprisingly well-separated. This result suggests that the three hydrophobic constructs apparently are more sensitive towards differences in the chemistry of the cell surfaces than to changes that result from the genotypic makeup of the cells. This finding is surprising, but it may be testimony that cancerous cells significantly change the makeup of the cell surface.

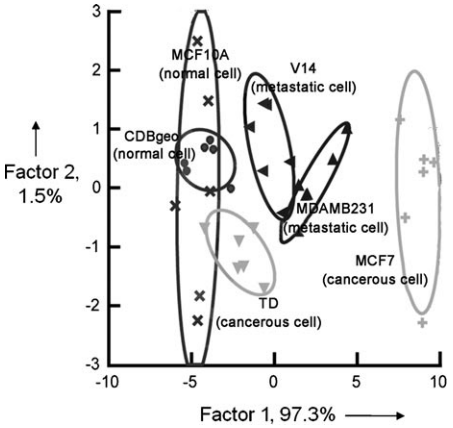

Figure 17. Canonical score plot for the first two factors of simplified fluorescence response patterns obtained with NP–PPE assembly arrays against different normal and cancerous breast cell types. Figure reproduced with permission from reference [36].

The presented method interestingly does not track cancer markers but rather detects subtle changes in the physical chemistry of the surfaces of the investigated cells. In the near future we plan to develop a reference database using different cancer cell types and record their interactions with a pool of NP–fluorophore constructs to explore potential clinical applications.

5. A Simple Pyrophosphate Sensor Using PPE–Spinel NP Constructs[37]

While gold NPs can be easily functionalized and are available in a variety of different flavors, other NPs might also be attractive as participants in IDA sensing. In the present case, 10 nm cobalt ferrite spinel nanocubes $(CoFe_2O_4)_n$ are readily synthesized using dimethylaminobenzoic acid (DMAB) as stabilizing ligand. Upon addition of PPE **2**, DMAB is displaced, and a self-assembled construct from **2** and the nanocubes forms, as determined by photoacustic IR experiments. A solution that is 5 μM in **2** lost 90% of its fluorescence in the presence of a 20 pM solution of nanocubes, thus suggesting vastly efficient binding. The absorption curves of the nanocubes overlap with the emission feature of **2**, likely leading to FRET, although electron-transfer quenching

mechanisms cannot be excluded. Figure 18 shows the principle of the complex formation, while Figure 19 displays emission spectra of **2** upon addition of nanocubes and the resulting Stern–Volmer type quenching curve.

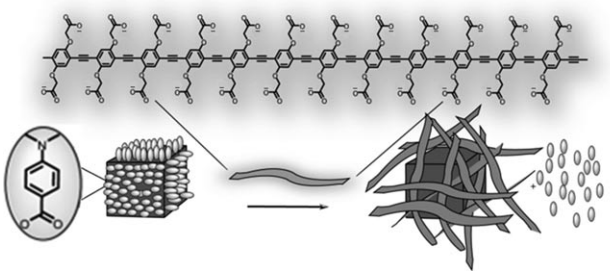

Figure 18. Schematic representation for the PPE–NP construct and fluorescence quenching with conjugated polymers. Displacement of the DMAB by **2** is shown. Figure reproduced with permission from reference [37].

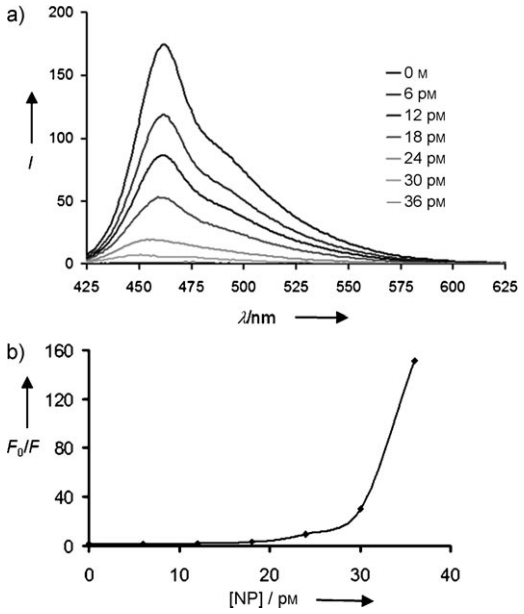

Figure 19. a) Fluorescence quenching of PPE **2** (5×10^{-6} M) by different concentrations of 10 nm NPs $(CoFe_2O_4)_x$ stabilized by DMAB and b) Stern–Volmer plot of the same system. The Stern–Volmer curve shows a fluorescence intensity ratio F_0/F, and the different absolute initial intensities as shown here have no bearing upon the Stern–Volmer plots, as they are, by definition, internally calibrated. Figure reproduced with permission from reference [37].

Metal oxide surfaces with exposed hydroxy groups and transition-metal cations can show strong interactions with small, hard inorganic oxo anions. In the case of the interaction of **2** with spinel nanocubes, phosphate-based anions had the largest effect upon the fluorescence restoration of bound **2**, while most other anions were not able to disrupt these constructs. Particularly interesting was the differentiation of phosphate (Pi) and pyrophosphate (PPi) by the constructs; visible fluorescence turn-on is effected by Pi at a level of 0.2 mM, while turn-on for PPi occurs at 2 μM. However, when using fluorescence spectroscopy, 40 nM PPi can be detected in a 0.1 mM solution of Pi. For potential diagnostic and biological applications, this result is important, as blood serum is millimolar in Pi, while the PPi concentration is micromolar. The serum ratio of Pi/PPi is greater than 250, and numerous cardiovascular and osteoporosis-related diseases are associated with an imbalance of Pi and PPi ratio.[38] The nanocube–PPE **2** constructs are useful as proof-of-concept sensors for this pair of anions, as they work in water and are easily assembled from inexpensive materials that can be made in large quantities. Further developments in selectivity and sensitivity are necessary to perform Pi/PPi sensing in serum or urine; however, these simple constructs are already surprisingly selective and sensitive when performing these measurements in buffer (Figure 20).

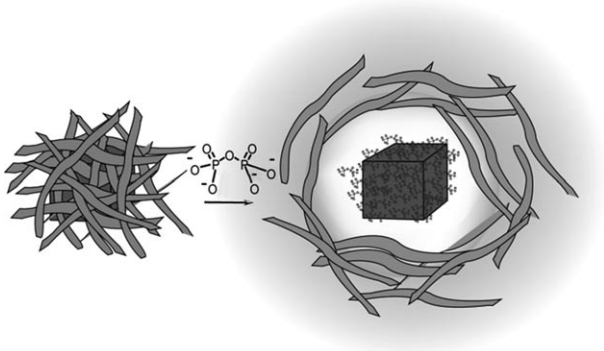

Figure 20. Working principle of the NP-based displacement assay. On the left-hand side is the quenched PPE–NP construct, and on the right-hand side is the now PPi-decorated NP and the displaced fluorescent PPE. Figure reproduced with permission from reference [37].

6. Conclusions

The combination of ammonium-functionalized 2 nm-core gold NPs with conjugated polymers or with green fluorescent protein in water gives rise to a diverse set[39] of self-assembled hydrophobic or electrostatic complexes or hybrids. Depending upon the ratio of conjugated polymer or GFP to gold NPs, the fluorescence of the construct can be precisely tuned; the higher the concentration of NPs, the lower the emission intensity. While the quenching mechanism is not fully understood, the overlap of the absorption spectrum of the gold NP with the emission spectra of the fluorophores suggests efficient energy-transfer quenching.

The formation of these "nonfluorescent" constructs is driven by electrostatic interactions, so that the ammonium head groups can carry a significant number of different substituents. The chemical nature of the used ammonium groups somewhat modulates the fluorescence quenching through the binding or association constants (K_a) between particle and fluorophore. However, regardless of the used NP, K_a is always high and averages between 10^7 and 10^{11} in water, with ammonium salts sporting aromatic head groups displaying the highest binding. The high K_a values allow for efficient assembly of the complexes at relatively low, analytically and

diagnostically relevant concentrations, with fluorophores in high nanomolar (100–500 nM) concentrations.

The interaction of the self-assembled hybrids with (negatively charged) biological analytes such as proteins in water or in serum, inorganic ions such as PPi, and bacterial or mammalian cells leads to a fluorescence modulation of the constructs; in most cases fluorescence turn-on results. In some cases, further additional quenching can be observed, perhaps by induced aggregation of the complexes or by analyte-induced aggregation of the involved fluorophores.

The salient and emergent, that is, not easily predictable, features of these hybrids are

- High selectivity for analyte groups when a small set of three to six NPs are used in combination with a suitable fluorophore to identify biological targets.
- Detection of very small amounts of added proteins to native human serum; that is, an excellent performance of the constructs in complex biological matrices.
- Detection and successful differentiation of proteins, bacteria, and cells by a small number of constructs.
- The above-stated feats are achieved by the exploitation of simple monolayer-protected gold NPs, positively charged, only showing differing but generic head groups, as shown in Figure 2.
- If more sophisticated head groups are used, the selectivity and the sensitivity of the employed NP–PPE constructs should be significantly increased over what we have reported to date. Potentially more sophisticated head groups include oligopeptides, sugars, small drug molecules or low-molecular-weight proteins that can be attached to the gold NP through the premade thiol–oligoethyleneglycol-type linkers that are used in the Rotello group.[18,22,23,32,36]

With little synthetic effort it should be possible to adapt the properties of the formed constructs to any need, increasing or decreasing K_a between NP and fluorophore and changing selectivity and sensitivity towards different analytes. At some point, with more sophisticated constructs, the sensitivity will only depend upon the amount of liberated fluorophore; at that point catalytic cycles will have to be considered, where a NP–catalyst complex might be used.

Combinations of simple ammonium-headgroup monolayer-functionalized NPs and polymeric and peptidic fluorophores detect and quantify proteins in water, buffer, and serum, but they can also distinguish between different bacterial strains and disease states in isogenic cell lines. Overall, this area might develop into a powerful low-tech complement to ELISA and antibody assays but also might be considered an upgraded, molecular version of gel electrophoresis. The limit of detection for various analytes can directly be managed by the structure of the constructs. For the detection of gross protein abnormalities in serum, our method is already competitive with the widely used simple electrophoretic methods.[1] The use of the NP–fluorophore constructs in clinical settings will depend upon their introduction into sufficiently simple and robust gadgets that do not necessitate a complex data workup but require only the addition of analyte to a solid-state strip or a simple microfluidic device. Only the surface of this method has been scratched with the experiments described in this Minireview.

The research was supported by the U.S. Department of Energy, Office of Basic Energy Sciences, Division of Materials Sciences and Engineering under Award DE-FG02-04ER46141 (U.B. summer salary; work in references [14b, 18, 19, 25a, 30b, 31, 32, 37] was completely or partially BES supported), the National Science Foundation (NSF) Center for Hierarchical Manufacturing at the University of Massachusetts (NSEC, DMI-0531171), and the NIH (GM077173 and AI073425).

Received: December 9, 2009
Published online: April 1, 2010

[1] R. A. McPherson, M. R. Pincus, *Henry's Clinical Diagnosis and Management by Laboratory Methods*, 21st Edition, Elsevier, Philadelphia, **2007**.
[2] F. Laure, C. Rouzioux, F. Veber, C. Jacomet, V. Courgnaud, S. Blanche, M. Burgard, C. Griscelli, C. Brechot, *Lancet* **1988**, *332*, 538–541.
[3] A. K. Deisingh, M. Thompson, *Analyst* **2002**, *127*, 567–581.
[4] a) K. Toko, *Sens. Actuators B* **2000**, *64*, 205–215; b) Y. Vlasov, A. Legin, *Fresenius J. Anal. Chem.* **1998**, *361*, 255–260; c) J. Janata, M. Josowicz, *Nat. Mater.* **2003**, *2*, 19–24.
[5] a) N. A. Rakow, K. S. Suslick, *Nature* **2000**, *406*, 710–713; b) C. Zhang, K. S. Suslick, *J. Am. Chem. Soc.* **2005**, *127*, 11548–11549; c) C. Zhang, K. S. Suslick, *J. Agric. Food Chem.* **2007**, *55*, 237–242.
[6] H. S. Hewage, E. V. Anslyn, *J. Am. Chem. Soc.* **2009**, *131*, 13099–13106.
[7] K. J. Albert, N. S. Lewis, C. L. Schauer, G. A. Sotzing, S. E. Stitzel, T. P. Vaid, D. R. Walt, *Chem. Rev.* **2000**, *100*, 2595–2626.
[8] a) N. T. Greene, K. D. Shimizu, *J. Am. Chem. Soc.* **2005**, *127*, 5695–5700; b) C. J. Stephenson, K. D. Shimizu, *Polym. Int.* **2007**, *56*, 482–488.
[9] a) M. Kitamura, S. H. Shabbir, E. V. Anslyn, *J. Org. Chem.* **2009**, *74*, 4479–4489; b) E. V. Anslyn, *J. Org. Chem.* **2007**, *72*, 687–699; c) B. T. Nguyen, E. V. Anslyn, *Coord. Chem. Rev.* **2006**, *250*, 3118–3127; d) A. T. Wright, E. V. Anslyn, *Chem. Soc. Rev.* **2006**, *35*, 14–28; e) S. L. Wiskur, P. N. Floriano, E. V. Anslyn, J. T. McDevitt, *Angew. Chem.* **2003**, *115*, 2116–2118; *Angew. Chem. Int. Ed.* **2003**, *42*, 2070–2072; f) S. L. Wiskur, H. Ait-Haddou, J. J. Lavigne, E. V. Anslyn, *Acc. Chem. Res.* **2001**, *34*, 963–972; g) T. S. Snowden, E. V. Anslyn, *Curr. Opin. Chem. Biol.* **1999**, *3*, 740–746.
[10] a) P. L. McGrier, K. M. Solntsev, S. Miao, L. M. Tolbert, O. R. Miranda, V. M. Rotello, U. H. F. Bunz, *Chem. Eur. J.* **2008**, *14*, 4503–4510; b) A. J. Zucchero, J. N. Wilson, U. H. F. Bunz, *J. Am. Chem. Soc.* **2006**, *128*, 11872–11881.
[11] M. C. Daniel, D. Astruc, *Chem. Rev.* **2004**, *104*, 293–346.
[12] a) N. L. Rosi, C. A. Mirkin, *Chem. Rev.* **2005**, *105*, 1547–1562; b) J. J. Storhoff, C. A. Mirkin, *Chem. Rev.* **1999**, *99*, 1849–1862.
[13] a) R. Shenhar, V. M. Rotello, *Acc. Chem. Res.* **2003**, *36*, 549–561; b) U. Drechsler, B. Erdogan, V. M. Rotello, *Chem. Eur. J.* **2004**, *10*, 5570–5579.
[14] a) M. Mammen, S. K. Choi, G. M. Whitesides, *Angew. Chem.* **1998**, *110*, 2908–2953; *Angew. Chem. Int. Ed.* **1998**, *37*, 2754–2794; b) I. B. Kim, B. Erdogan, J. N. Wilson, U. H. F. Bunz, *Chem. Eur. J.* **2004**, *10*, 6247–6254.
[15] a) A. Verma, V. M. Rotello, *Chem. Commun.* **2005**, 303–312; b) L. L. Kiessling, N. L. Pohl, *Chem. Biol.* **1996**, *3*, 71–77; c) J. E.

Gestwicki, C. W. Cairo, L. E. Strong, K. A. Oetjen, L. L. Kiessling, *J. Am. Chem. Soc.* **2002**, *124*, 14922 – 14933.
[16] C. Fan, S. Wang, J. W. Hong, G. C. Bazan, K. W. Plaxco, A. J. Heeger, *Proc. Natl. Acad. Sci. USA* **2003**, *100*, 6297 – 6301.
[17] Q. Zhou, T. M. Swager, *J. Am. Chem. Soc.* **1995**, *117*, 12593 – 12602.
[18] R. L. Phillips, O. R. Miranda, D. E. Mortenson, C. Subramani, V. M. Rotello, U. H. F. Bunz, *Soft Matter* **2009**, *5*, 607 – 612.
[19] I. B. Kim, A. Dunkhorst, J. Gilbert, U. H. F. Bunz, *Macromolecules* **2005**, *38*, 4560 – 4562.
[20] H. Jiang, P. Taranekar, J. R. Reynolds, K. S. Schanze, *Angew. Chem.* **2009**, *121*, 4364 – 4381; *Angew. Chem. Int. Ed.* **2009**, *48*, 4300 – 4316.
[21] J. C. Ma, D. A. Dougherty, *Chem. Rev.* **1997**, *97*, 1303 – 1324.
[22] C. C. You, O. R. Miranda, B. Gider, P. S. Ghosh, I. B. Kim, B. Erdogan, S. A. Krovi, U. H. F. Bunz, V. M. Rotello, *Nat. Nanotechnol.* **2007**, *2*, 318 – 323.
[23] M. De, S. Rana, H. Akpinar, O. R. Miranda, R. R. Arvizo, U. H. F. Bunz, V. M. Rotello, *Nat. Chem.* **2009**, *1*, 461 – 465.
[24] H. J. Issaq, Z. Xiao, T. D. Veenstra, *Chem. Rev.* **2007**, *107*, 3601 – 3620.
[25] a) I. B. Kim, A. Dunkhorst, U. H. F. Bunz, *Langmuir* **2005**, *21*, 7985 – 7989; b) C. E. Halkyard, M. E. Rampey, L. Kloppenburg, S. L. Studer-Martinez, U. H. F. Bunz, *Macromolecules* **1998**, *31*, 8655 – 8659.
[26] H. J. Issaq, T. D. Veenstra, T. P. Conrads, D. Felschow, *Biochem. Biophys. Res. Commun.* **2002**, *292*, 587 – 592.
[27] a) V. Berry, A. Gole, S. Kundu, C. J. Murphy, R. F. Saraf, *J. Am. Chem. Soc.* **2005**, *127*, 17600 – 17601; b) C. R. Bertozzi, M. D. Bednarski, *J. Am. Chem. Soc.* **1992**, *114*, 2242 – 2245 .
[28] C. C. Lin, Y. C. Yeh, C. Y. Yang, C. L. Chen, G. F. Chen, C. C. Chen, Y. C. Wu, *J. Am. Chem. Soc.* **2002**, *124*, 3508 – 3509.
[29] R. S. Norman, J. W. Stone, A. Gole, C. J. Murphy, T. L. Sabo-Atwood, *Nano Lett.* **2008**, *8*, 302 – 306.
[30] a) M. D. Disney, J. Zheng, T. M. Swager, P. H. Seeberger, *J. Am. Chem. Soc.* **2004**, *126*, 13343 – 13346; b) I. B. Kim, J. N. Wilson, U. H. F. Bunz, *Chem. Commun.* **2005**, 1273 – 1275.
[31] R. L. Phillips, I. B. Kim, B. E. Carson, B. Tidbeck, Y. Bai, T. L. Lowary, L. M. Tolbert, U. H. F. Bunz, *Macromolecules* **2008**, *41*, 7316 – 7320.
[32] R. L. Phillips, O. R. Miranda, C. C. You, V. M. Rotello, U. H. F. Bunz, *Angew. Chem.* **2008**, *120*, 2628 – 2632; *Angew. Chem. Int. Ed.* **2008**, *47*, 2590 – 2594.
[33] D. C. Oliveira, H. de Lencastre, *Antimicrob. Agents Chemother.* **2002**, *46*, 2155 – 2161.
[34] M. S. Maynor, T. L. Nelson, C. O'Sullivan, J. J. Lavigne, *Org. Lett.* **2007**, *9*, 3217 – 3220.
[35] B. S. Reisner, G. L. Woods, *J. Clin. Microbiol.* **1999**, *37*, 2024 – 2026.
[36] A. Bajaj, O. R. Miranda, I. B. Kim, R. L. Phillips, D. J. Jerry, U. H. F. Bunz, V. M. Rotello, *Proc. Natl. Acad. Sci. USA* **2009**, *106*, 10912 – 10916.
[37] I. B. Kim, M. H. Han, R. L. Phillips, B. Samanta, V. M. Rotello, Z. J. Zhang, U. H. F. Bunz, *Chem. Eur. J.* **2009**, *15*, 449 – 456.
[38] a) E. Chantelau, *VASA-J. Vascular Diseases* **2001**, *30*, 15 – 20; b) H. Fleisch, R. G. Russell, F. Straumann, *Nature* **1966**, *212*, 901 – 903.
[39] R. Hoffmann, *Angew. Chem.* **2001**, *113*, 3439 – 3443; *Angew. Chem. Int. Ed.* **2001**, *40*, 3337 – 3340.